



Comparative photocatalytic degradation of two dyes on immobilized TiO₂ nanoparticles: Effect of dye molecular structure and response surface approach

M. Fathinia, A.R. Khataee*, M. Zarei, S. Aber

Department of Applied Chemistry, Faculty of Chemistry, University of Tabriz, Tabriz, Iran

ARTICLE INFO

Article history:

Received 18 August 2010

Received in revised form

25 September 2010

Accepted 28 September 2010

Available online 14 October 2010

Keywords:

TiO₂ nanoparticles

Photocatalysis

Immobilization

Experimental design

Decolorization

ABSTRACT

In this work, comparative photocatalytic degradation of an anionic dye (C.I. Acid Blue 92 (AB92)) and a cationic dye (C.I. Basic Blue 3 (BB3)) under UV light irradiation using supported TiO₂ nanoparticles in a rectangular photoreactor was studied. The investigated TiO₂ was Millennium PC-500 (crystallites mean size 8 nm and surface area of 320.76 m²/g) immobilized on glass plates. Response surface methodology (RSM) was employed to assess individual and interactive effects of the four main independent parameters (initial dye concentration, UV light intensity, flow rate and reaction time) on the decolorization efficiency. Central composite design was used for optimization of UV/TiO₂ process. Predicted values of decolorization efficiency were found to be in good agreement with experimental values for AB92 and BB3 ($R^2 = 0.9435$ and $Adj-R^2 = 0.8941$, $R^2 = 0.9309$ and $Adj-R^2 = 0.8704$, respectively). Optimization results showed that maximum decolorization efficiency was achieved at the optimum conditions: initial dye concentration 10 mg/L, UV light intensity 47.2 W/m², flow rate 100 mL/min and reaction time 200 min. Photocatalytic mineralization of the dyes was monitored by total organic carbon (TOC) decrease. The degradation pathway of AB92 was proposed based on the identified compounds by GC–Mass technique.

© 2010 Elsevier B.V. All rights reserved.

1. Introduction

Dyeing and finishing of textile goods is a major environmental concern, because of the introduction of large quantities of color, chemical oxygen demand, non-biodegradable organics and other hazardous chemicals into the process effluents [1]. In recent years, various technologies have been developed for environmental pollutants remediation [2]. In general, the treatment of dye-containing effluents is being undertaken by biological, adsorption, membrane, coagulation–flocculation, oxidation–ozonation and advanced oxidation processes (AOPs) [3–6]. AOPs involve generation and subsequent reaction of hydroxyl radicals •OH and can be used for the complete mineralization of many pollutants, like pesticides, pharmaceuticals, and dyes [7–10]. Heterogeneous photocatalysis via combination of TiO₂ and UV light is considered one of the most promising AOPs for destruction of water-soluble organic pollutants [11,12]. In the literature reports, the most widely used photocatalytic process is carried out in a batch slurry photoreactor operating with titanium dioxide suspensions [11–13]. However, slurry reactors have a number of practical and economical disadvantages. The main problem related to suspended photocatalyst systems is the separation of TiO₂ nanoparticles after treatment

[5,11]. Moreover, the recent studies have raised concerns about the potential toxicity of titanium dioxide nanoparticles [14]. In addition, the depth of penetration of UV light in the suspended photocatalyst systems is limited because of the strong light absorption by the catalyst particles. In order to solve these problems, immobilized photocatalysts have been developed. The most important properties of a suitable support are to be chemically inert, to present a high specific surface area and to be transparent to UV radiation [14–16]. In the present work, TiO₂ nanoparticles were fixed on the sandblasted glass plates by sol–gel dip-coating method.

The photocatalytic decolorization efficiency in continuous reactors is dependent on a number of parameters such as the reactor configuration, initial dye concentration, UV light intensity, flow rate, reaction time and molecular structure of the dye. In the conventional methods used to determine the influence of operational parameters, experiments were carried out varying systematically the studied parameter and keeping constant the others. This should be repeated for all the influencing parameters, resulting in an unreliable number of experiments. To optimize the effective parameters with the minimum number of experiments, the application of experimental design methodologies can be useful. Response surface methodology (RSM) is a statistical method being useful for the optimization of chemical reactions and/or industrial processes and widely used for experimental design [17]. In this technique, the main objective is to optimize the response surface that is influenced by process parameters. RSM also quantifies the relationship between the controllable input parameters and the obtained

* Corresponding author. Tel.: +98 411 3393165; fax: +98 411 3340191.

E-mail addresses: a.khataee@tabrizu.ac.ir, ar.khataee@yahoo.com (A.R. Khataee).

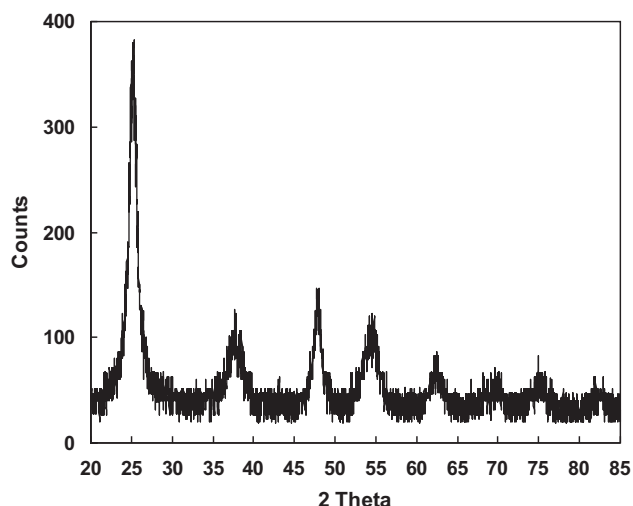


Fig. 1. X-ray diffraction pattern of TiO₂ PC-500.

response surfaces [18]. Process optimization by RSM is faster for gathering experimental research results than the rather conventional, time consuming one-factor-at-a-time approach [18].

In our previous work, we have studied optimization of photocatalytic degradation of C.I. Basic Blue 3 (BB3) under UV light irradiation using TiO₂ nanoparticles immobilized on non-woven paper [19]. The present work is focused on the comparative photocatalytic degradation of an anionic and a cationic dye with different molecular structures using glass plates as a support of TiO₂ nanoparticles. The central composite design (CCD) has been applied to the optimization of photocatalytic treatment of the dye solutions on the immobilized TiO₂ nanoparticles in a rectangular photocatalytic reactor. The factors (variables) investigated were the reaction time, initial dye concentration, flow rate and UV light intensity. The photocatalytic degradation compounds formed in this process were analyzed by GC–Mass technique. In addition, total organic carbon (TOC) removal was monitored in order to explain the mineralization of the dye in the UV/TiO₂ process.

2. Experimental

2.1. Materials

The investigated photocatalyst was Millennium TiO₂ PC-500 (anatase >99%, crystallites mean size 8 nm) immobilized on glass plates. These characteristics were proved by our XRD and TEM analyses which have been shown in Figs. 1 and 2. BET surface area and total pore volume of the used photocatalyst were 320.76 m²/g and 0.3104 cm³/g, respectively. The dyes, C.I. Acid Blue 92 and C.I. Basic Blue 3 were obtained from Shimi Boyakhsaz Company (Iran), their chemical structure and characteristics are given in Table 1. Methanol, methyltrimethoxysilane (MTMOS), HCl and N,O-bis-(trimethylsilyl)acetamide were obtained from Merck Co. (Germany).

2.2. Immobilization of TiO₂ nanoparticles on glass plates

TiO₂ nanoparticles were fixed on the sandblasted glass plates by sol–gel dip-coating method. Organically modified silica (Ormosil) was used as hydrophobic binder. The coating solution contained 23 mL of methanol, 0.264 g of TiO₂ nanoparticles, and appropriate amount of methyltrimethoxysilane (MTMOS), which was set to achieve the desired TiO₂/Ormosil weight ratio. HCl solution (1 N) was added for hydrolysis of MTMOS. The suspension was sonicated for 15 min by a Sonoplus Ultrasonic Homogenizer HD 2200

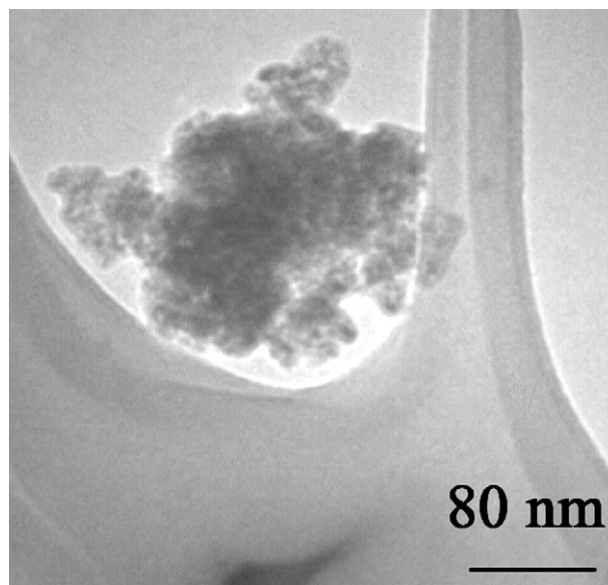


Fig. 2. Transmission electron microscopy image of TiO₂ PC-500.

(Germany). The main advantage of this kind of films is that they have good mechanical anchoring due to the chemical bonding, in comparison with films made with the dried mixture of TiO₂ and water. Fig. 3 shows the SEM images of the glass plate before and after immobilization of TiO₂ nanoparticles on it. Two interaction types between TiO₂ surface and MTMOS under anhydrous (a) and hydrous conditions (b) have been shown in Fig. 4. It is well

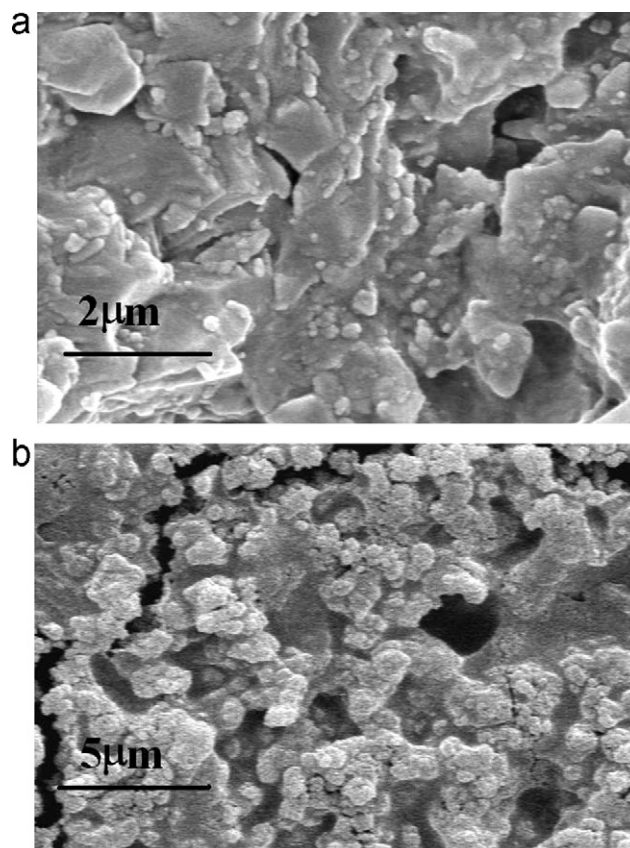
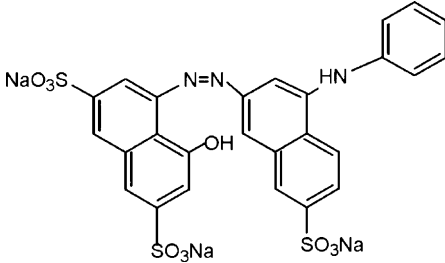
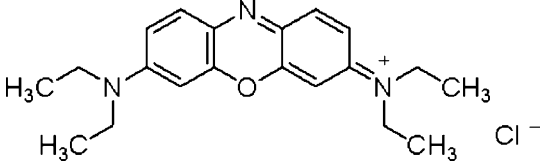


Fig. 3. Scanning electron microscopy images of TiO₂ nanoparticles (a) before and (b) after deposition on glass plates.

Table 1
Structure and characteristics of the three commercial dyes.

Color index name	C.I. Acid Blue 92 (AB92)	C.I. Basic Blue 3 (BB3)
Chemical structure		
Chemical class	Anionic, Monoazo	Cationic, Monoxazine
Molecular formula	C ₂₆ H ₁₆ N ₃ Na ₃ O ₁₀ S ₃	C ₂₀ H ₂₆ N ₃ OCl
Color index number	13390	51004
λ _{max} (nm)	571	654
M _w (g/mol)	695.58	359.89

known that silane coupling agents (MTMOS) are firstly hydrolyzed to silanols in hydrous conditions (see Fig. 4b) [20], and then firstly a condensation reaction between the silanols and surface hydroxyl groups of TiO₂ nanoparticles occurs. Secondly, the condensation reaction between the surface modified TiO₂ nanoparticles and pretreated glass plates occurs. The immobilized TiO₂ nanoparticles possess the high firmness to the support due to the presence of chemical bonds between TiO₂ nanoparticles and pretreated glass plates. Three kinds of interaction between silane coupling agents (MTMOS), hydroxyl groups of TiO₂ and pretreated glass plates, which have been shown in Fig. 4b are (a) hydrogen bonding, (b) proton transfer following the condensation reaction, and (c) covalent siloxane bond between hydroxyl groups of TiO₂ and hydroxyl groups of pretreated glass plates via silane coupling agents [20].

2.3. Photocatalysis experiments

The experimental set-up is based on a rectangular photocatalytic reactor with workable area of 15 cm × 90 cm, made out of stainless steel that its schematic diagram and function were explained previously [19]. 2000 mL solutions of AB92 and BB3 were degraded in all cases. Artificial irradiation was provided by three 30 W UV-C lamps (Philips, the Netherlands) with peak intensity at 254 nm, positioned above the reactor. The lamps were turned on at the beginning of each experiment. The distance between the solution and the UV source was adjusted according to the experimental conditions. On the surface of the solution, the radiation intensity was measured by Cassy Lab (Germany). At different reaction times obtained with experimental design, 2 mL sample was taken and the remaining dye was determined using the calibration curves at λ_{max} of the dyes. Using this method, the percentage of color removal could be obtained. The percent color removal (CR (%)) was expressed as the percentage ratio of decolorized dye concentration to that of the initial one.

2.4. Analytical procedures

The photocatalytic reactions were monitored by UV–Vis spectrophotometer (WPA lightwave S2000, England) in the range of 200–800 nm. Scanning electron microscopy (SEM) was carried out on a Hitachi SEM (Model S-4160, USA) device after gold-plating of the samples. The samples used for transmission electron microscopy (TEM) observations were prepared by dispersing the TiO₂ powder in ethanol followed by ultrasonic vibration (Sonorex Bandelin Digi Tec, UK) for 15 min, then placing a drop of the dispersion onto a copper grid coated with a layer of amorphous

carbon. TEM was carried out on a Zeiss EM 900, Germany. To determine the crystal phase composition and average crystalline size of immobilized TiO₂ nanoparticles sample, X-ray diffraction (XRD) measurements were carried out at room temperature by using Siemens X-ray diffraction D5000, with Cu Kα radiation. The accelerating voltage of 40 kV and emission current of 30 mA were used. The average crystalline size of the catalyst was calculated according to Debye–Scherrer formula [21]. It can be observed from Fig. 1 that the peaks in XRD are at 2θ = 25.3°, 37.8°, and 48.1°, which correspond to anatase form TiO₂. Nitrogen sorption analyses were obtained with a (Micrometrics, Gemini series) sorptometer using standard continuous procedures at 77.15 K on calcined samples that had been degassed at 363 K for 1 h and then at 403 K under high vacuum for at least 10 h. The surface area was calculated according to the Brunauer–Emmett–Teller (BET) model over a relative pressure range of 0.05–0.90. Total organic carbon (TOC) measurements were carried out by TOC analyzer of Shimadzu TOC-VCSH (North America).

For GC–Mass analysis, an Agilent 6890 gas chromatograph with a 30 m to 0.25 mm HP-5MS capillary column coupled with an Agilent 5973 mass spectrometer (Agilent Technologies, Palo Alto, Canada) operating in EI mode at 70 eV was used. To identify the aromatic intermediates, 2000 mL solution containing 20 mg/L of AB92 at optimized conditions was treated for 10, 30 and 120 min. The resulted solution was saturated with Na₂SO₄, before the extraction of organic components with 30 mL of diethyl ether three times. The collected organic solution was evaporated and the remaining solid was dissolved in 100 μL of N,O-bis-(trimethylsilyl)acetamide under heating at 60 °C and stirring for 10 min. The resulting silylated products were then analyzed by GC–Mass by the following temperature program: 50 °C for 4 min, 8 °C min⁻¹ up to 300 °C and hold time of 4 min. The temperature of the inlet, transfer line and detector was 250, 250 and 300 °C, respectively [4].

2.5. Experimental design

In the present study central composite design, which is a widely used form of RSM, was employed for optimization and comparison of photocatalytic decolorization of an anionic dye (AB92) and a cationic dye (BB3). In order to evaluate the influence of operating parameters on the photocatalytic decolorization efficiency of AB92 and BB3, four main factors were chosen: initial dye concentration (mg/L) (X₁), UV light intensity (W/m²) (X₂), flow rate (mL/min) (X₃) and reaction time (min) (X₄). A total of 31 experiments were employed in this work for each dye, including 2⁴ = 16 cube points, 7 replications at the center point and 8 axial points. Experimental

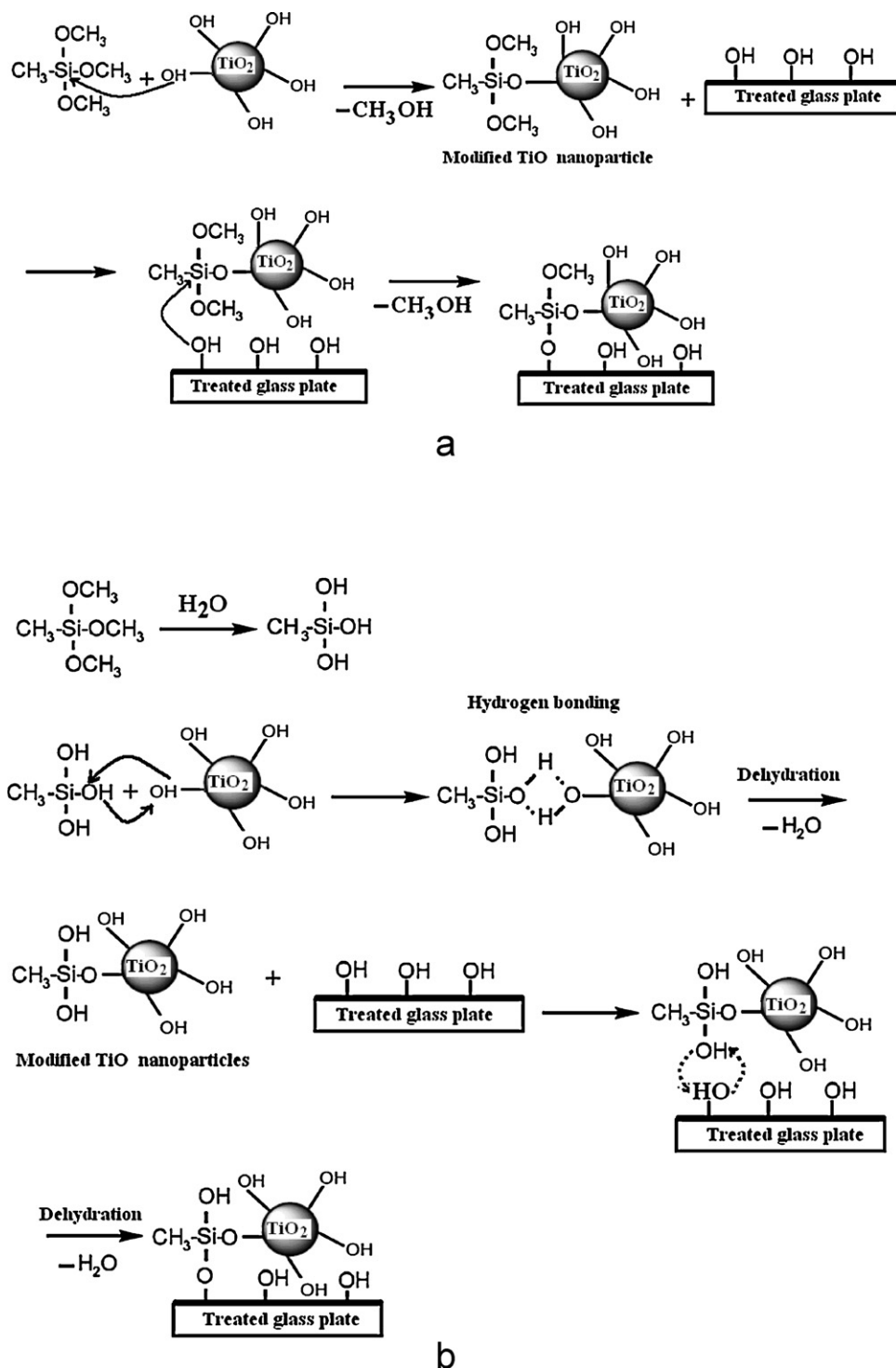


Fig. 4. The proposed mechanism for immobilization of TiO_2 nanoparticles on glass plates in anhydrous (a) and hydrous conditions (b).

data were analyzed using Minitab 15 software. For statistical calculations, the variables X_i were coded as x_i according to the following equation:

$$x_i = \frac{X_i - X_0}{\delta X} \quad (1)$$

where X_0 is the value of X_i at the center point and δX presents the step change [22,23]. The experimental ranges and the levels of the independent variables for both dyes removal are given in Table 2. It should be mentioned that preliminary experi-

ments were performed to determine the extreme values of the variables.

3. Results and discussion

3.1. CCD model and residuals analysis

The 4-factor CCD matrix and experimental results obtained in the photocatalytic decolorization runs are presented in Table 3. The second-order polynomial response equation (Eq. (2)) was used to

Table 2
Experimental ranges and levels of the independent test variables.

Variables	Ranges and levels				
	−2	−1	0	+1	+2
Initial dye concentration (mg/L) (X_1)	2	6	10	14	18
UV light intensity (W/m^2) (X_2)	12.2	20.95	29.70	38.45	47.20
Flow rate (mL/min) (X_3)	50	100	150	200	250
Reaction time (min) (X_4)	40	90	140	190	240

correlate the dependent and independent variables:

$$Y = b_0 + b_1x_1 + b_2x_2 + b_3x_3 + b_4x_4 + b_{12}x_1x_2 + b_{13}x_1x_3 + b_{14}x_1x_4 + b_{23}x_2x_3 + b_{24}x_2x_4 + b_{34}x_3x_4 + b_{11}x_1^2 + b_{22}x_2^2 + b_{33}x_3^2 + b_{44}x_4^2 \quad (2)$$

where Y is the response variable of decolorization efficiency. The b_i s are regression coefficients for linear effects; b_{ik} the regression coefficients for quadratic effects and x_i represent coded experimental levels of the variables.

Based on these results, an empirical relationship between the response and independent variables was attained and expressed by the following second-order polynomial equation for AB92 (Y_1) and BB3 (Y_2), respectively:

$$Y_1 = 52.6043 - 4.3767x_1 + 6.5392x_2 + 2.4525x_3 + 11.9692x_4 + 2.0158x_1x_2 + 2.4433x_1x_3 + 0.1108x_1x_4 - 3.5267x_2x_3 + 1.1750x_2x_4 + 0.2400x_3x_4 + 0.4100x_1^2 - 0.0462x_2^2 + 0.0063x_3^2 - 0.5337x_4^2 \quad (3)$$

$$Y_2 = 52.8929 - 8.1440x_1 + 4.6240x_2 + 3.5735x_3 + 11.9692x_4 + 2.9388x_1x_2 + 0.0601x_1x_3 - 0.3862x_1x_4 - 1.4237x_2x_3 - 1.4748x_2x_4 + 1.2348x_3x_4 - 0.8977x_1^2 + 1.0889x_2^2 - 0.4861x_3^2 + 1.4186x_4^2 \quad (4)$$

Photocatalytic decolorization efficiencies (CR (%)) have been predicted by Eqs. (3) and (4) and presented in Table 3. These results indicated good agreements between the experimental and predicted values of decolorization efficiency. The correlation coefficient (R^2) quantitatively evaluates the correlation between the experimental data and the predicted responses. The experimental results and the predicted values obtained from the model (Eqs. (3) and (4)) were compared. It was found that the predicted values matched the experimental values reasonably well with $R^2 = 0.9435$ and $R^2 = 0.9309$ for AB92 and BB3, respectively. This implies that 94.35% and 93.09% of the variations for AB92 and BB3 percent color removal are explained by the independent variables and this also means that the model does not explain only about 5.65% and 6.91% of variation. Adjusted R^2 (Adj- R^2) is also a measure of goodness of a

Table 3
The 4-factor central composite design matrix and the value of response function (CR (%)).

Run	[Dye] ₀ (mg/L)	Intensity (W/m^2)	Flow rate (mL/min)	Time (min)	Decolorization efficiency (%)			
					Experimental		Predicted	
					AB92	BB3	AB92	BB3
1	0	−2	0	0	53.98	50.82	49.30	43.89
2	0	0	−2	0	48.31	48.24	48.14	44.20
3	+2	0	0	0	49.59	40.48	51.91	48.36
4	−1	+1	−1	+1	70.56	72.47	73.32	75.83
5	−1	−1	−1	+1	59.95	63.42	62.49	66.78
6	−1	−1	+1	+1	60.69	67.95	65.94	72.12
7	−1	+1	+1	−1	50.91	56.35	54.52	57.99
8	0	0	0	0	48.50	52.15	52.60	52.89
9	0	0	0	−2	17.19	26.01	14.56	23.32
10	+1	+1	+1	+1	69.96	73.28	71.48	66.96
11	−1	−1	−1	−1	36.50	36.34	38.31	42.98
12	0	0	0	0	56.26	52.31	52.60	52.89
13	−2	0	0	0	78.49	91.89	69.42	80.94
14	+1	−1	+1	+1	54.85	58.33	56.13	59.45
15	0	0	+2	0	64.53	57.53	57.95	58.50
16	−1	−1	+1	−1	39.75	38.91	43.90	42.64
17	+1	+1	−1	−1	43.33	37.91	41.42	34.06
18	−1	+1	−1	−1	47.00	52.33	49.12	53.97
19	0	0	0	0	52.10	53.41	52.60	52.89
20	0	0	0	0	52.02	56.55	52.60	52.89
21	0	0	0	+2	66.55	71.46	62.44	71.07
22	−1	+1	+1	+1	73.95	85.06	76.59	85.52
23	+1	−1	+1	−1	31.88	36.61	32.46	33.56
24	+1	−1	−1	+1	52.00	50.50	51.72	49.18
25	0	+2	0	0	77.52	58.52	75.46	62.38
26	+1	−1	−1	−1	25.14	26.66	25.91	28.96
27	0	0	0	0	57.65	50.55	52.60	52.89
28	+1	+1	−1	+1	68.00	53.29	67.26	52.32
29	0	0	0	0	52.87	51.92	52.60	52.89
30	0	0	0	0	48.83	53.36	52.60	52.89
31	+1	+1	+1	−1	46.91	43.61	47.78	43.01

Table 4
Analysis of variance (ANOVA) for fit of decolorization efficiency from central composite design.

Source of variations	Regression		Residuals		Total	
	AB92	BB3	AB92	BB3	AB92	BB3
Sum of squares	5815.54	6300.64	348.10	468.02	6163.64	6768.66
Degree of freedom	14	14	16	16	30	30
Adjusted mean square	415.40	450.05	21.76	29.25		
F-value	19.09	15.39				

AB92: $R^2 = 0.9435$, $\text{Adj-}R^2 = 0.8941$.

BB3: $R^2 = 0.9309$, $\text{Adj-}R^2 = 0.8704$.

fit, but it is more suitable for comparing models with different numbers of independent variables. It corrects R^2 -value for the sample size and the number of terms in the model by using the degrees of freedom on its computations. If there are many terms in a model and not very large sample size, $\text{Adj-}R^2$ may be visibly smaller than R^2 [24,25]. Here, $\text{Adj-}R^2$ values for AB92 and BB3 (0.8941, 0.8704) were very close to the corresponding R^2 value (see Table 4).

In addition to correlation coefficient, the adequacy of the models was also evaluated by the residuals (difference between the observed and the predicted response value). Residuals are thought as elements of variation unexplained by the fitted model and then it is expected that they occur according to a normal distribution. Normal probability plots are a suitable graphical method for judging residuals normality. The observed residuals are plotted against the expected values, given by a normal distribution (see Fig. 5a and b) for AB92 and BB3, respectively. Trends observed in Fig. 5a and b reveal reasonably well-behaved residuals. Based on this plots, the residuals appear to be randomly scattered.

Table 4 indicates the results of the quadratic response surface model fitting in the form of analysis of variance (ANOVA). ANOVA is required to test the significance and adequacy of the model [26,27]. ANOVA subdivides the total variation of the results into two components: variation associated with the model and variation associated with the experimental error, showing whether the variation from the model is significant or not when compared with the ones associated with residual error [23,24,26]. This comparison is performed by F -value, which is the ratio between the mean square of the model and the residual error. If the model is a good predictor of the experimental results, F -value should be greater than the tabulated value of F -distribution for a certain number of degrees of freedom in the model at a level of significance α . F -value obtained for AB92 and BB3 19.09 and 15.39, are clearly greater than the tabulated F (2.352 at 95% significance) confirming the adequacy of the model fits.

The student's t distribution and the corresponding values, along with the parameter estimate, are given in Table 5 for AB92 and BB3. The P -values were used as a tool to check the significance of each of the coefficients, which in turn, are necessary to understand the pattern of the mutual interactions between the test variables. The larger the magnitude of the student's t -test and smaller P -value, the more significant is the corresponding coefficient [26,27].

The Pareto analysis gives more significant information to interpret the results. In fact, this analysis calculates the percentage effect of each factor on the response, according to the following relation [28,29]:

$$P_i = \left(\frac{b_i^2}{\sum b_i^2} \right) \times 100 \quad (i \neq 0) \quad (5)$$

Fig. 6a and b shows the Pareto graphic analysis of AB92 and BB3, respectively. As can be seen in these figures among the variables, reaction time (b_4 , 60.82, 54.44%) and UV light intensity (b_2 , 18.15, 25.34%) produce the main effects on photocatalytic decolorization efficiency of AB92 and BB3, respectively.

3.2. Effect of variables as response surface and counter plots

To study the effect of initial dye concentration on photocatalytic decolorization efficiency of AB92 and BB3, the experiments were carried out with initial dyes concentration varying from 2 to 18 mg/L at constant flow rate (150 mL/min) and UV light intensity (29.7 W/m²). The results have been displayed for AB92 and BB3 in Fig. 7a and b, respectively. These figures show that the photocatalytic decolorization efficiency slightly decreases with an increase in the initial amount of AB92 and BB3. This may be attributed to several factors. At high dye concentration, the adsorbed dye molecules may occupy all the active sites of TiO₂ surface and this leads to decrease in degradation efficiency. It means that as the concentration of the dye increases, more and more molecules of the dye get adsorbed on the surface of the photocatalyst. Therefore, requirement of the reactive species ($\bullet\text{OH}$ and $\bullet\text{O}_2^-$) needed for the degradation of the dye also increase. However, the formation of $\bullet\text{OH}$ and $\bullet\text{O}_2^-$ on the catalyst surface remains constant for a given light intensity, catalyst amount and duration of irradiation. Hence, the available hydroxyl radicals are inadequate for the degradation of the dye at high concentrations. Consequently, the degradation efficiency of the dye decreases as the concentration increases [30,31]. In addition an increase in substrate concentration can lead to the generation of intermediates, which may adsorb on the surface of the catalyst. Slow diffusion of the generated intermediates from the catalyst surface can result in the deactivation of active sites of the photocatalyst and consequently, a reduction in the degradation efficiency. In contrast, at low concentration, the number of the catalytic sites will not be limiting factor and the rate of degradation is proportional to the substrate concentration [32]. Another reason may be due to the absorption of light photon by the dye itself leading to a lesser availability of photons for hydroxyl radical generation [11,33].

Fig. 8a and b illustrates the effect of UV light intensity and reaction time on photocatalytic decolorization efficiency for initial dye concentration of 10 mg/L and flow rate of 150 mL/min. As it is obvious from Fig. 8, decolorization efficiency increases with increasing UV light intensity and reaction time. The reason of this observation is thought to be the fact that UV light intensity determines the extent of light absorption by the photocatalyst to form electron-hole pairs which results in the overall pollutant conversion. In other words, higher light intensity provides higher energy for more TiO₂ nanoparticles to produce electron-hole pairs [34].

Fig. 9 shows the response surface and contour plots of photocatalytic decolorization efficiency as a function of flow rate and reaction time. A slightly improvement in photocatalytic decolorization efficiency with increasing flow rate has been observed. The presumed reason is that when the dye solution flow rate is increased, the turbulence in the system is enhanced. It may lead to decompose more and more adsorbed dye molecules on the surface of TiO₂ thus photocatalytic decolorization efficiency increases. The higher decolorization efficiencies at higher flow rates are also attributed to the increase in the mass transfer coefficient [35].

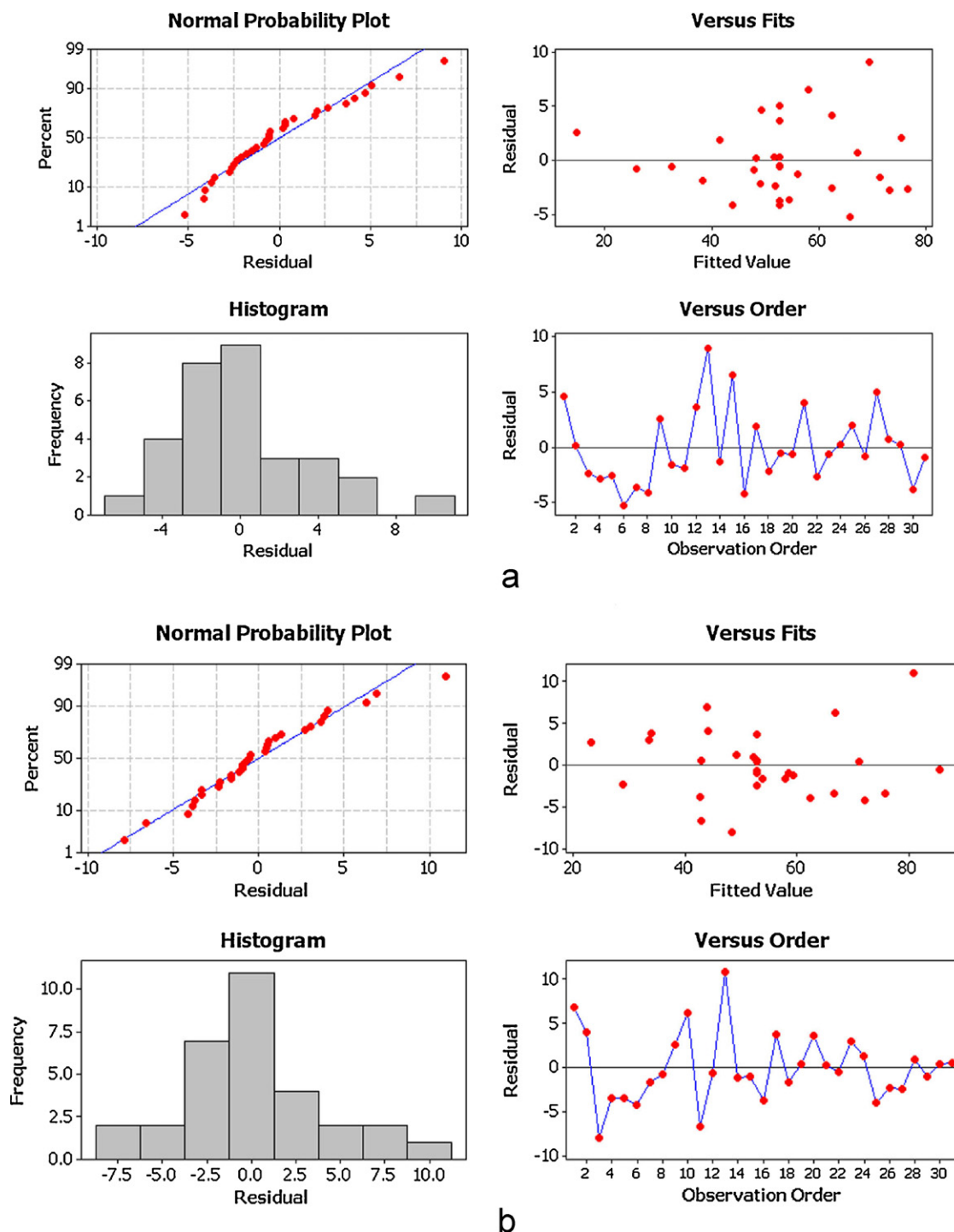


Fig. 5. Residual plots for photocatalytic destruction efficiency of (a) AB92 and (b) BB3.

3.3. Determination of optimal conditions for photocatalytic removal of the dyes

The main objective of the optimization in this work is to determine the optimum values of variables for photocatalytic decolorization process, from the model obtained using experimental data. The desired goal in terms of decolorization efficiency was defined as “maximize” to achieve highest treatment performance. The optimum values of the process variables for the maximum decolorization efficiency were 10 mg/L, 47.2 W/m², 100 mL/min and 200 min for initial dyes concentration (X_1), UV light intensity

(X_2), flow rate (X_3) and reaction time (X_4), respectively which has been shown in Table 6. At these optimum values, the predicted and observed CR (%) was 78.36 and 80.35% for AB92 and 65.65 and 63.36% for BB3, respectively. It implies that the strategy to optimize the decolorization conditions and to obtain the maximal decolorization efficiency by RSM for photocatalytic decolorization of AB92 and BB3 in this study is successful. Photocatalytic mineralization of the dyes in UV/TiO₂ process was studied with 20 mg/L of AB92 and BB3 solutions by TOC loss. The results indicated that 100% TOC removal was achieved under optimized conditions at the irradiation time of 12 h.

Table 5
Estimated regression coefficients and corresponding *t* and *P* values from the data of central composite design experiments.

Coefficient	Parameter estimate		Standard error		<i>t</i> -value		<i>P</i> -value	
	AB92	BB3	AB92	BB3	AB92	BB3	AB92	BB3
b_0	52.604	52.893	1.763	2.044	29.839	25.875	0.000	0.000
b_1	-4.377	-8.144	0.952	1.104	-4.597	-7.377	0.000	0.000
b_2	6.539	4.624	0.952	1.104	6.868	4.188	0.000	0.001
b_3	2.453	3.573	0.952	1.104	2.576	3.237	0.020	0.005
b_4	11.969	11.937	0.952	1.104	12.571	10.812	0.000	0.000
b_{12}	2.016	2.939	0.872	1.011	2.311	2.906	0.034	0.010
b_{13}	2.443	0.060	0.872	1.011	2.801	0.059	0.013	0.953
b_{14}	0.111	-0.386	0.872	1.011	0.127	-0.382	0.900	0.708
b_{23}	-3.527	-1.424	0.872	1.011	-4.043	-1.408	0.001	0.178
b_{24}	1.175	-1.475	1.166	1.352	1.008	-1.091	0.329	0.292
b_{34}	0.240	1.235	1.166	1.352	0.206	0.913	0.840	0.375
b_{11}	0.410	-0.898	1.166	1.352	0.352	-0.664	0.730	0.516
b_{22}	-0.046	1.089	1.166	1.352	-0.040	0.805	0.969	0.432
b_{33}	0.006	-0.486	1.166	1.352	0.005	-0.359	0.996	0.724
b_{44}	-0.534	1.419	1.166	1.352	-0.458	1.049	0.653	0.310

3.4. Effect of the dye molecular structure on photocatalysis efficiency

The results reported in Table 6, indicated that the photocatalytic decolorization efficiency of AB92 was higher than that of BB3 at the optimized conditions. This result is in accordance with the

results of Epling and Lin study [36]. On the other hand, at other than optimized conditions the photocatalytic activity of BB3 is higher than AB92 which confirms the results of Rauf and Ashraf work [37]. The chemical structure of the organic dyes has a considerable effect on the photocatalytic reactivity. This effect has been explored by different researchers. Epling and Lin [36] have eval-

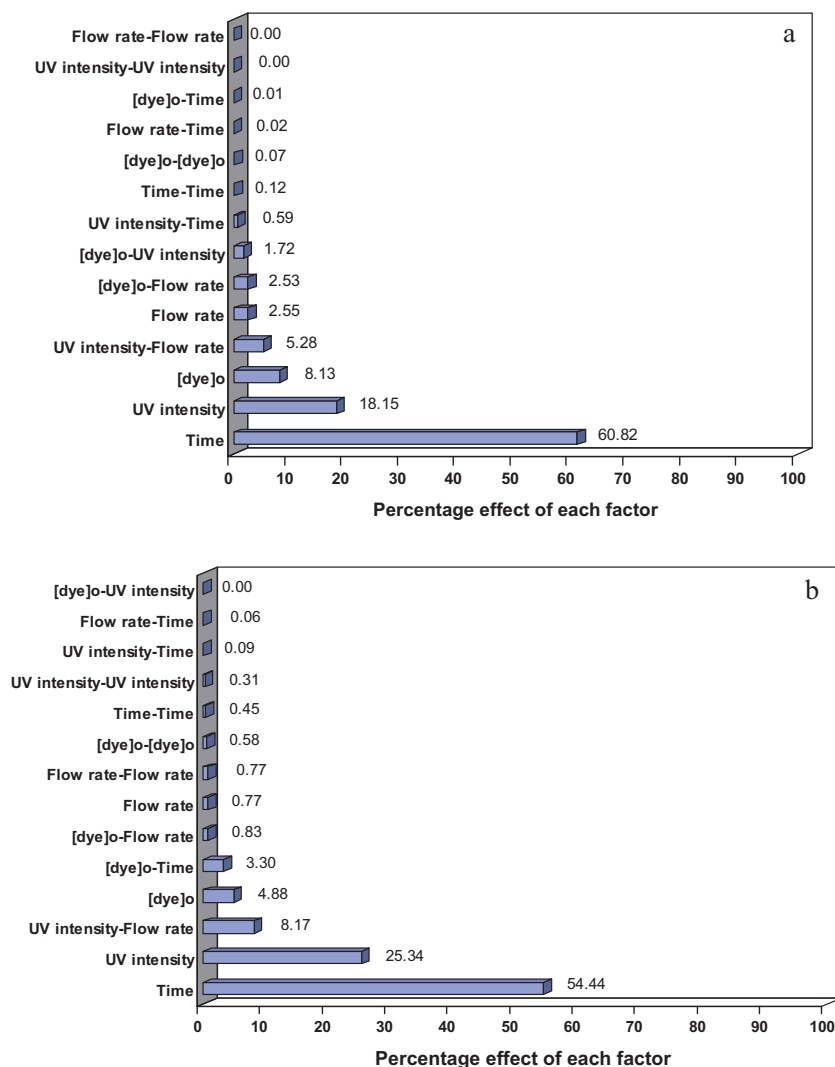


Fig. 6. Pareto graphic analysis of (a) AB92 and (b) BB3.

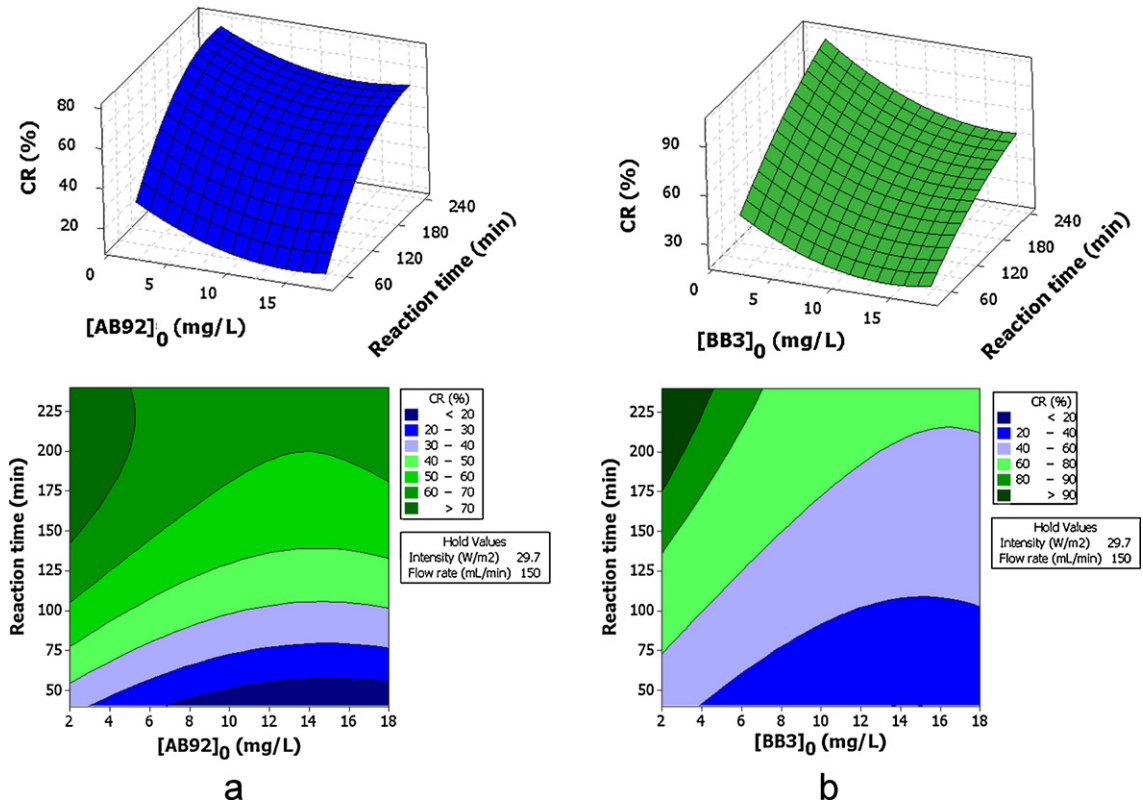


Fig. 7. The response surface and contour plots of photocatalytic decolorization efficiency (%) as the function of reaction time (min) and initial dye concentration (mg/L) of (a) AB92 and (b) BB3.

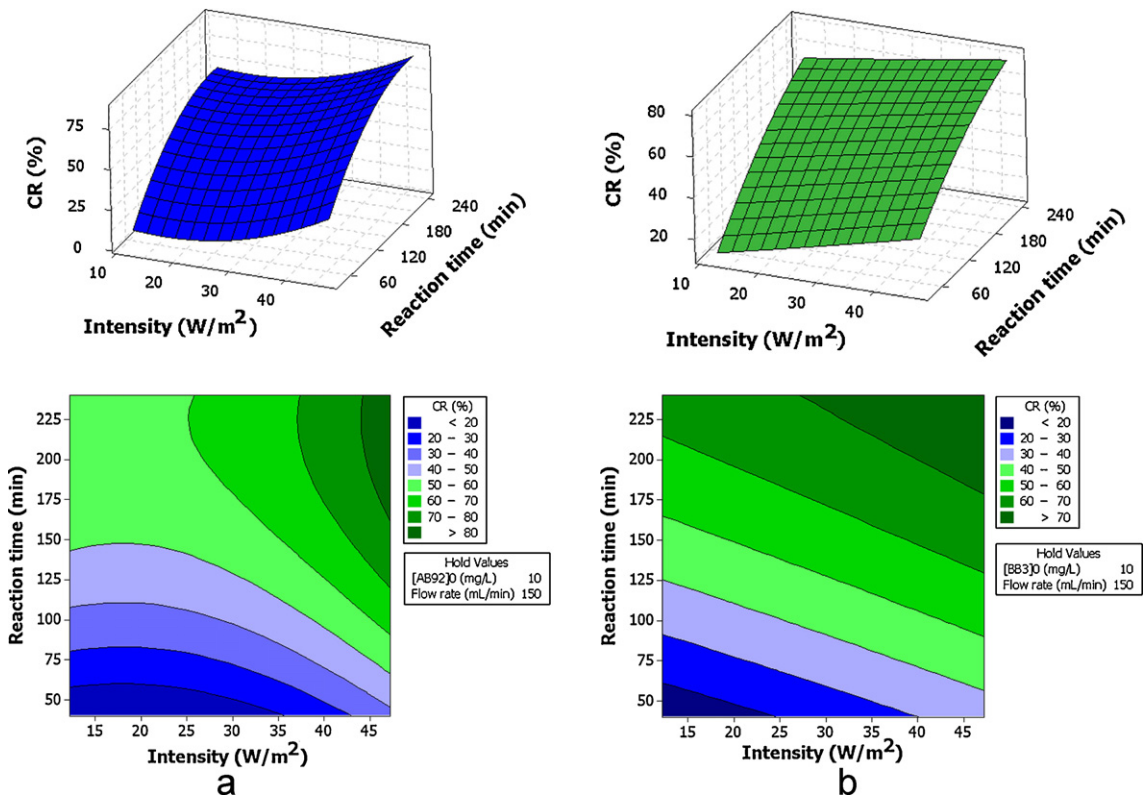


Fig. 8. The response surface and contour plots of photocatalytic decolorization efficiency (%) as the function of (b) reaction time (min) and UV light intensity (W/m²) (mg/L) of (a) AB92 and (b) BB3.

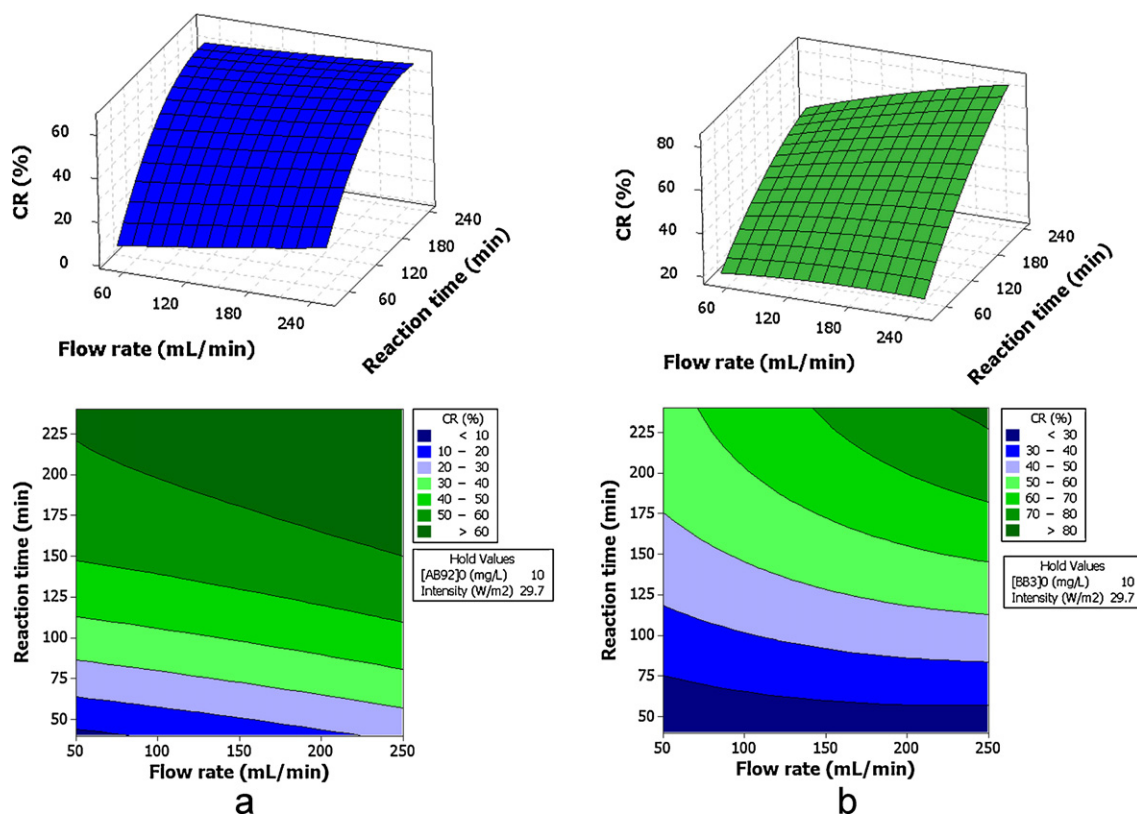


Fig. 9. The response surface and contour plots of photocatalytic decolorization efficiency (%) as the function of reaction time (min) and flow rate (mL/min) of (a) AB92 and (b) BB3.

uated the visible light assisted degradation of a range of dyes and concluded that anionic food dyes degraded at a faster rate compared to the cationic and neutral dyes. In contrast, Rauf and Ashraf [37] showed that the cationic dyes degraded at a faster rate compared to anionic dyes. They also reported that diaryl methane and anthraquinonic dyes exhibited the fastest and the slowest degradation rates, respectively. Anionic dyes are widely used to color natural fibers like cotton, wool, silk, paper and leather, which are hydrophilic in nature, and are also used in food, drugs, cosmetics and inks [38]. In this study, we have chosen an anionic dye (AB92) that belongs to monoazo class by functionality. This class of dyes contains an azo group ($-N=N-$) in their molecular structure. Cationic dyes are used for synthetic fibers such as modified nylon, polyester and acrylics [38]. In this study, we have chosen BB3 as a cationic dye, which belongs to oxazin class by functionality. This class of dyes is heteropolyaromatic containing more than one (usually two) heteroatom (N, O or S) at the central benzene ring. The mechanism of the photocatalytic reaction may depend on the adsorption ability of the degraded compound on the surface of TiO_2 . One of the factors that affect the extent of the dye adsorption is the charge of the dye molecule. Since the charge depends on the

Table 6
Optimum operating conditions of the process variables.

Variable	Optimum value	
	AB92	BB3
Initial dye concentration (mg/L) (X_1)	10	10
UV light intensity (W/m^2) (X_2)	47.2	47.2
Flow rate (mL/min) (X_3)	100	100
Reaction time (min) (X_4)	200	200
Experimental CR (%)	78.36	63.36
Predicted CR (%)	80.35	65.64

pH of solution, it is expected both pH and the nature of the dye influence the photocatalyst activity [39].

The pH value of AB92 and BB3 solutions in this work was 5.8–6. According to the point of zero charge of TiO_2 ($pzc = 6.2$), its surface is presumably positively charged in acidic solution and negatively charged in alkaline solution [31]. Since AB92 has a sulfonic group in its structure, these negatively charged groups favors adsorption of dye onto photocatalyst surface, thus the photodegradation efficiency increases [31].

On the other hand in comparison to BB3, the azo group of AB92 is susceptible to be attacked by hydroxyl radicals that make AB92 to degrade easily [40,36]. Another structural difference between the two dyes is the presence of hydroxyl group ($-OH$) in the structure of AB92. The presence of hydroxyl groups in the dye molecule can intensify its resonance and consequently the degradation efficiency [40]. In terms of the functional group effects, the presence of electron withdrawing groups in the structure of dyes was observed to retard the degradation efficiency. The presence of electron withdrawing group $=N(C_2H_5)_2$ in the structure of BB3 retards the photocatalytic degradation efficiency. Surprisingly, the presence of the electron withdrawing sulfonic group in AB92 makes it only very slightly less sensitive to oxidation. Indeed, molecules with one, two or three sulfonic functions have almost the same reactivity with respect to oxidation by hydroxyl radicals [40]. AB92, containing three sulfonic groups, showed higher photocatalytic reactivity in comparison with that of BB3 which contains no sulfonic substituent. In fact, study of the influence of the sulfonic group is difficult, because this substituent operates in different fields: it decreases electron density in the aromatic rings and the β nitrogen atom of the azo bond. On the other hand, it increases the hydrophilic–lipophilic balance of the dye molecules, and consequently slows down their aggregation degree [40].

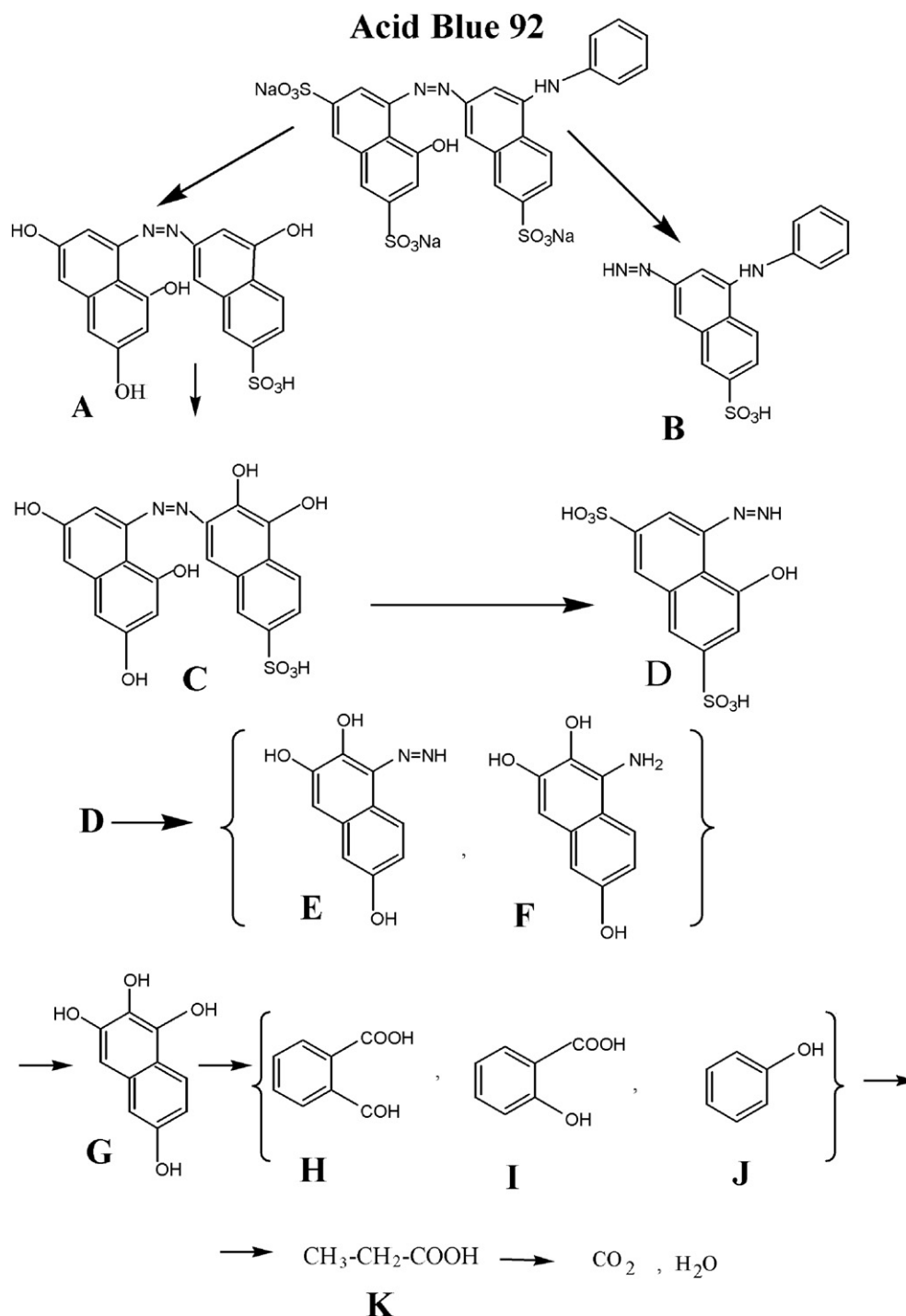


Fig. 10. Proposed photocatalytic degradation pathway of AB92.

3.5. Photocatalytic degradation pathway of AB92

In our previous work, we have studied intermediates that were generated through photocatalytic degradation of BB3 using TiO_2 nanoparticles immobilized on non-woven paper [19]. The present work is focused on the intermediates generated during the photocatalytic degradation process of AB92. The generated intermediates analyzed by GC–MS and identified by comparison with commercial standards and by interpretation of their fragment ions in the mass spectra. It has been attempted to identify the main aromatic metabolites resulting from AB92 decomposition. The intermediates are presented in Fig. 10, where they are logically reported according

to their decreasing molecular weight. As it was reported in Table 7, eleven compounds were successfully detected (A, B, C, D, E, F, G, H, I, J, and K). It should be pointed out that other than the compounds successfully detected, several other chromatographic peaks were also found but could not be positively identified (i.e. the match factor of the mass spectrum was below 90%). It is obvious that as soon as the aromatic rings of AB92 were opened a wide range of cleavage compounds are expected. Unfortunately, such by-products could not be detected due to the limitations associated with the employed analytical technique or they were not significantly accumulated in the medium. On the other hand, some of intermediates have not been identified, probably because in case of their generation, they

Table 7
Identified aromatic by-products during photocatalytic process.

Compound ^b	Retention time (min)	Main fragments
A	26.68	429, 377, 341, 281, 253, 147
B	9.87	329, 304, 214, 147, 93, 73
C	26.68	445, 405, 341, 281, 207
D	26.37	341, 281, 253, 207, 73
E	4.06	204, 171, 147, 73
F	9.87	190, 147, 114, 73, 51
G	3.59	190, 169, 147, 116, 73
H	2.65	182, 147, 110, 73, 53 ^a
I	5.45	181, 140, 99, 73 ^a
J	3.59	116, 95, 73, 53 ^a
K	3.39	117, 95, 73, 53 ^a

^a Value corresponding to the trimethylsilyl derivative.

^b See Fig. 10 for the respective compounds.

are quickly oxidized to their derivatives. Fig. 10 shows a plausible general reaction mechanism sequence for the photocatalytic degradation of AB92 based on the compounds identified by GC–MS in this work. The azo linkage of AB92 was first reduced to hydrogenated azo structure without destroying benzene rings and naphthalene rings, product (B). In the photooxidation treatment, hydrogenated azo linkage was broken and substituted benzene and naphthalene were produced, they can be further oxidized and finally mineralized to produce carbon dioxide. The two transformation products (C, D) were detected, and can be postulated to be formed via a cleavage of C–N bond with the detachment of the amino benzene and SO_3^- , and insertion of an $\bullet\text{OH}$ group. The formation of (E, F) from (D) suggests the reductive cleavage of the azo group prior to the opening of the aromatic ring. The products (I, J, K) that were detected can be postulated to be formed via hydroxylation of substituted benzene and naphthalene group. The naphthalene group can be subjected by $\bullet\text{OH}$ radicals and consequently the corresponding phenolic compounds can be formed which are spontaneously oxidized into acids such as benzoic acid, butendioic acid and other short-chain acids that are converted directly into CO_2 (see Fig. 10).

4. Conclusions

The photocatalytic treatment of a textile dyes, an anionic dye (AB92) and a cationic dye (BB3), from aqueous solution in a rectangular photocatalytic reactor was optimized. The effect of dye molecular structure on photocatalytic degradation was discussed. The effect of operational parameters on the decolorization efficiency of AB92 and BB3 was evaluated by the response surface and contour plots. The optimum values of the initial dye concentration, UV light intensity, flow rate and reaction time were 10 mg/L, 47.2 W/m², 100 mL/min, 200 min, respectively. At the optimum conditions the experimental and predicted decolorization efficiencies for AB92 and BB3 were 78.36, 80.35% and 63.36, 65.64%, respectively. Analysis of variance showed a high coefficient of determination for AB92 and BB3 ($R^2 = 0.9435, 0.9309$ and $\text{Adj-}R^2 = 0.8941, 0.8704$, respectively), thus ensuring a satisfactory adjustment of the second order regression model with the experimental data. The results of TOC decrease and GC–Mass analysis indicated that photocatalytic process can be used for complete decolorization and mineralization of both dyes. The intermediate compounds of AB92 degradation were identified and the relevant pathway was proposed.

Acknowledgements

The authors thank the University of Tabriz, Iran for financial and other supports. We also sincerely thank Water and Wastewater Company of East Azerbaijan for TOC analysis.

References

- [1] N.H. Ince, Water Res. 33 (1999) 1080–1084.
- [2] F. Thevenet, O. Guaitela, J.M. Herrmann, A. Rousseau, C. Guillard, Appl. Catal. B: Environ. 61 (2005) 58–68.
- [3] J.W. Shi, S.H. Chen, S.M. Wang, P. Wu, G.H. Xu, J. Mol. Catal. A: Chem. 303 (2009) 141–147.
- [4] A.R. Khataee, G. Dehghan, A. Ebadi, M. Zarei, M. Pourhassan, Bioresour. Technol. 101 (2010) 2252–2258.
- [5] A.R. Khataee, V. Vantanpour, A.R. Amani, J. Hazard. Mater. 161 (2009) 1225–1233.
- [6] A. Aleboye, M.B. Kasiri, M.E. Olya, H. Aleboye, Dyes Pigments 77 (2008) 288–294.
- [7] S. Chiron, A. Fernandez-Alba, A. Rodriguez, E. Garcia-Calvo, Water Res. 34 (2000) 366–377.
- [8] L.A. Pérez-Estrada, S. Malato, W. Gernjak, A. Agüera, E.M. Thurman, I. Ferrer, A.R. Fernández-Alba, Environ. Sci. Technol. 39 (2005) 8300–8306.
- [9] M.S. Lucas, J.A. Peres, Dyes Pigments 71 (2006) 236–244.
- [10] M.M. Ballesteros Martín, J.A. Sánchez Pérez, J.L. Casas López, I. Oller, S. Malato Rodríguez, Water Res. 43 (2009) 653–660.
- [11] N. Daneshvar, D. Salari, A.R. Khataee, J. Photochem. Photobiol. A: Chem. 162 (2004) 317–322.
- [12] M. Karkmaz, E. Puzeat, C. Guillard, J.M. Herrmann, Appl. Catal. B: Environ. 51 (2004) 183–194.
- [13] J.M. Herrmann, Top. Catal. 34 (2005) 49–65.
- [14] G. Falck, H. Lindberg, S. Suhonen, M. Vippola, E. Vanhala, J. Catalán, K. Savolainen, H. Norppa, Hum. Exp. Toxicol. 28 (2009) 339–352.
- [15] A. Alinsafi, F. Evenou, E.M. Abdulkarim, M.N. Pons, O. Zahraa, A. Benhammou, A. Yaacoubi, A. Nejmeddine, Dyes Pigments 74 (2007) 439–445.
- [16] A. Aguedach, S. Brosillon, J. Morvan, E.K. Lhadi, J. Hazard. Mater. 150 (2008) 250–256.
- [17] R.H. Myers, D.C. Montgomery, Response Surface Methodology: Process and Product Optimization using Designed Experiments, 2nd ed., John Wiley & Sons, USA, 2002.
- [18] N. Aslan, Powder Technol. 185 (2008) 80–86.
- [19] A.R. Khataee, M. Fathinia, S. Aber, M. Zarei, J. Hazard. Mater. 181 (2010) 886–897.
- [20] T. Jeisonowski, A. Krysztalkiewicz, Appl. Surf. Sci. 171 (2001) 18–32.
- [21] A.L. Patterson, Phys. Rev. 56 (1939) 978–982.
- [22] A.R. Khataee, Environ. Technol. 31 (2010) 73–86.
- [23] A. Aleboye, N. Daneshvar, M.B. Kasiri, Chem. Eng. Process. 47 (2008) 827–832.
- [24] S.C.R. Santos, R.A.R. Boaventura, Appl. Clay Sci. 42 (2008) 137–145.
- [25] G.E.P. Box, D.W. Behnken, J. Technometrics 2 (1960) 455–475.
- [26] M. Zarei, D. Salari, A. Niaei, A.R. Khataee, J. Hazard. Mater. 173 (2010) 544–551.
- [27] H.L. Liu, Y.R. Chiou, Chem. Eng. J. 112 (2005) 173–179.
- [28] D.P. Haaland, Experimental Design in Biotechnology, Marcel Dekker, Inc., New York, Basel, 1989.
- [29] A. Kesraoui-Abdessaïem, N. Oturan, N. Bellakhal, M. Dachraoui, M.A. Oturan, Appl. Catal. B: Environ. 78 (2008) 334.
- [30] W. Bahnemann, M. Muneer, M.M. Haque, Catal. Today 124 (2007) 133–148.
- [31] N. Daneshvar, D. Salari, A.R. Khataee, J. Photochem. Photobiol. A: Chem. 157 (2003) 111–116.
- [32] K. Selvam, M. Muruganandham, I. Muthuvel, M. Swaminathan, Chem. Eng. J. 128 (2007) 51–57.
- [33] R.A. Damodar, J.T. Swaminathan, Sol. Energy 81 (2007) 1–7.
- [34] A.E. Cassano, O.M. Alfano, Catal. Today 58 (2000) 167–197.
- [35] M.F.J. Dijkstra, H.J. Pannemana, J.G.M. Winkelmana, J.J. Kellyb, A.A.C.M. Beenackers, Chem. Eng. Sci. 57 (2002) 4895–4907.
- [36] G.A. Epling, C. Lin, Chemosphere 46 (2002) 561–570.
- [37] M.A. Rauf, S.S. Ashraf, Chem. Eng. J. 151 (2009) 10–18.
- [38] K. Hunger (Ed.), Industrial Dyes—Chemistry, Properties, Applications, Wiley-VCH, Weinheim, 2003.
- [39] U.G. Akpan, B.H. Hameed, J. Hazard. Mater. 170 (2009) 520–529.
- [40] A.R. Khataee, M.B. Kasiri, J. Mol. Catal. A: Chem. 328 (2010) 8–26.